Appl Magn Reson (2016) 47:925–935
DOI 10.1007/s00723-016-0801-9

Applied
Magnetic Resonance

Zinc–Nickel Ferrite Nanoparticles as a Contrast Agent in Magnetic Resonance Imaging

N. Sattarahmady[1,2] · M. Heidari[1] · T. Zare[1] · M. Lotfi[3] · H. Heli[1]

Received: 30 April 2016 / Revised: 22 May 2016 / Published online: 2 June 2016

Abstract Today, contrast agents are used to improve the sensitivity of magnetic resonance imaging (MRI) to detect pathologic structures. Ferrite nanoparticles are a class of superparamagnetic contrast agents in MRI. In this study, $Zn_{0.5}Ni_{0.5}Fe_2O_4$ nanoparticles were synthesized via precipitation method and coated with dextrin to increase the solubility and biocompatibility. The morphology, size, structure, and magnetic properties of nanoparticles were investigated. These nanoparticles have superparamagnetic property with a narrow size distribution with a mean diameter of about 20.5 ± 3.2 nm. MRI study using phantom agar shows that these nanoparticles can be used as an effective contrast agent for T_2 and T_2^*-weighted imaging. The relaxivities of r_2 and r_2^* are 8.78 and 82.08 s^{-1} mmol L^{-1}, respectively. From these findings, it is possible that dextrin-coated $Zn_{0.5}Ni_{0.5}Fe_2O_4$ nanoparticles can be used as a good negative contrast agent in MRI.

1 Introduction

Magnetic resonance imaging (MRI) is one of the non-invasive and informative techniques with high resolution in diagnostic medicine. However, the difference between the contrast of the images of normal and abnormal tissues is not always sufficient. Using an effective contrast agent, the contrasting of this modality is significantly enhanced [1–3].

✉ H. Heli
hheli7@yahoo.com; heli@sums.ac.ir

[1] Nanomedicine and Nanobiology Research Center, Shiraz University of Medical Sciences, Shiraz, Iran

[2] Department of Medical Physics, School of Medicine, Shiraz University of Medical Sciences, Shiraz, Iran

[3] Department of Radiology, Shiraz University of Medical Sciences, Shiraz, Iran

In the past decade, nanoparticles are of intense current interest from fundamental scientific studies to miniaturization of devices, and for a variety of applications in magnetic storage media [4], energy storage devices [5, 6], sensing and biosensing [7–11], and medicine [12–14], due to their physical properties vary dramatically from their bulk counterparts arising from their small size. In particular, magnetic nanoparticles (MNPs) of small size, with the properties of non-toxicity, biocompatibility, injectability, and high-level of accumulation in the target tissue or organ, are attracted in biomedical applications [1, 15, 16]. These particles are—attracting materials as contrast agents of MRI. They cause negative contrast in MRI by reducing the signal intensity of T_2-weighted images [1, 17]. T_1 and T_2 relaxation times are characterized as longitudinal or spin–lattice relaxation, and transverse or spin–spin relaxation, respectively [2]. Relaxivity is obtained by measuring the contrast agent concentration dependency of the relaxation rates ($1/T_1$ and $1/T_2$) [18]. Relaxation increment due to non-homogeneity in the magnetic field or tissue-contrast agents interface is reflected in the transverse relaxation time T_2^* [18]. Based on the magnetic properties, the current contrast agents are classified as superparamagnetic and paramagnetic materials, and according to the magnitude of their relaxivities r_1 and r_2, they are described as T_1- or T_2-imaging agents [19, 20]. Efficiency of negative contrast agents, such as superparamagnetic iron oxide nanoparticle (SPION), for ultra-sensitive imaging and shortening T_2 and T_2^* arises from their ultra-small hydrodynamic size and large magnetic moment [2, 21, 22].

Superparamagnetic behavior of SPIONs is reduced upon aggregation, and the reticular endothelial system can capture these aggregate forms [23]. Coating of SPIONs by polymeric shells prevents the aggregation and enhances the biocompatibility for in vivo employments [24, 25]. Up to now, various polymers [26], surfactants [27], and proteins [28] were employed for coating contrast agents. Starch-based materials, such as dextrin, due to their biodegradable property, are proper for coating contrast agents [29, 30].

Ferrite nanoparticles (NPs) with the MFe_2O_4 formula (M is a divalent metal ion) have received a lot of attention due to their low saturation magnetic moments [31], electrical properties, thermal stability, and ability to manipulate chemically with relatively inert properties [32]. Ferrite NPs have been employed in biomedical applications, such as magnetic extraction, MRI, cell labeling, biosensors, drug delivery, and hyperthermia [16, 33]. Ferrite NPs have been suggested as T_2 MRI contrast agents [22, 34].

In this study, dextrin-coated zinc–nickel ferrite ($Zn_{0.5}Ni_{0.5}Fe_2O_4$) NPs (d-NFNPs) were synthesized, characterized, and evaluated as a contrast agent in MRI.

2 Experimental Section

2.1 Materials

All chemicals were purchased from Merck (Germany) or Scharlau (Spain) and used without further purification.

2.2 Synthesis of Dextrin-Coated d-NFNPs

d-NFNPs were synthesized by an aqueous precipitation technique. Briefly, the individual metal chloride salts, in the appropriate stoichiometric proportions, were dissolved in a diluted hydrochloric acid (0.1 mol L^{-1}) solution and heated to 80 °C. A solution containing sodium hydroxide (4 mol L^{-1}) and dextrin (12.5 g L^{-1}) was prepared separately and heated to 80 °C. These hot solutions were then rapidly mixed with magnetic stirring (final mixture pH of 12.0). The temperature was then increased to 100 °C, and stirring was continued for further 1 h. This time is needed for crystallization of the ferrite NPs. Then, the solution was cooled naturally, and the precipitate was collected by a permanent magnet and washed several times with distilled water to neutralize the supernatant. The samples were dried at room temperature for further use.

2.3 Characterization

The crystal structure of d-NFNPs was identified using a Philips X'Pert diffractometer (the Netherlands) equipped with a Cu/K_α radiation source ($\lambda = 0.1540$ nm) at a scanning rate of 1° min^{-1} in the 2θ range from 5° to 100°. Atomic force microscopy (AFM) was performed by a Nano Wizard 108 II, JPK instrument (Germany) in non-contact mode to evaluate the structure and size of d-NFNPs. A Zeiss, Sigma-IGMA/VP field emission scanning electron microscope (Germany) and a Philips CM30 transmission electron microscope were employed to study the particle size and surface morphology. Coating the $Zn_{0.5}Ni_{0.5}Fe_2O_4$ NPs (NFNPs) surface was investigated using a Fourier transform infrared (FTIR) instrument, Bruker Tensor 27 spectrometer (Germany). The magnetic properties of dried d-NFNPs were measured using a vibrating sample magnetometer (VSM; Meghnatis Daghigh Kavir Co. (Iran) at room temperature. The external magnetic field varied from −20 to 20 kOe.

2.4 Magnetic Resonance Relaxivity Study Using a Phantom

Agarose phantom was used for evaluating d-NFNPs as a T_2 and T_2^*-weighted MRI contrast agent. For this purpose, different concentrations of d-NFNPs (0.05, 0.175, 0.250, 0.425, and 0.500 μg mL^{-1}) were suspended in a 1 % (w/v) agarose gel in a 96-well ELISA plate. The plate was embedded in a water tank and inserted into an MRI knee coil. T_2 and T_2^*-weighted MRI images were obtained using a 1.5-T Magnetom Avanto, Siemens MR instrument (Germany) with turbo spin–echo pulse sequence. Eight different times of spin echo (TE) from 22 to 98 ms were used for T_2 determination with the time of repetition (TR) = 1800 ms. Scan parameters were set as follows: field of view (FOV) = 160 × 160 mm^2 and slice thickness = 3 mm. For T_2^* determination, eight different gradient-echo-TEs were used ranging from 11 to 39 ms, with TR = 350 ms, FOV = 160 × 160 mm^2, slice thickness = 3 mm. Other parameters were matrix = 320 × 256 and flip angle (FA) = 30°. The values of r_2 and r_2^* were calculated by the curve fitting of plots of $1/T_2$ and $1/T_2^*$ (in s^{-1})

versus the sum of the concentration (in mmol L^{-1}) of nickel and iron species in the d-NFNPs.

3 Results

An X-ray diffraction (XRD) pattern of d-NFNPs is shown in Fig. 1. The spectrum includes characteristic peaks at 2θ of about 31°, 36°, 37°, 43°, 54°, 57°, 63°, and 74°. The pattern of the diffractogram is according to the nickel ferrite (JCPDS card number 74–2081). These diffractions are assigned to (2 2 0), (3 1 1), (2 2 2), (4 0 0), (4 2 2), (5 1 1), (4 4 0), and (5 3 3) reflection planes, respectively. These correspond to pure nickel ferrite phase of spinel cubic structure with a space group fd3 m. Also, the mean crystalline size of NFNPs was obtained as 6.3 ± 1.4 nm, based on the full width at half maximum of diffraction peaks using the Scherrer equation.

Figure 2 shows a field emission scanning electron microscopy (FESEM) (a) and transmission electron microscopy (TEM) (b, c) images of d-NFNPs. d-NFNPs have spherical morphology and are agglomerated due to their magnetic property. For further analysis of the size and morphology of d-NFNPs, an AFM image was recorded, as shown in Fig. 3. In this image, the NPs are relatively agglomerated and formed particles with a mean size of 20.5 ± 3.2 nm. This ultra-small size will be advantageous for biological applications.

Magnetic properties of d-NFNPs were evaluated by a vibrating sampling magnetometer at room temperature, and its magnetic hysteresis loop is shown in Fig. 4. The hysteresis loop is lacking, and the coercitive field and remanent magnetization values are almost equal to zero. These indicate superparamagnetic behavior of the sample, which is important for biomedical using. The saturated magnetization (M_s) value is obtained as 12.3 emu g^{-1}.

The magnetic moment per formula unit in Bohr magneton for d-NFNPs was calculated from saturation magnetization of the hysteresis loop using the following equation [35]:

$$n_B = (M_w M_s)/5585 \quad (1)$$

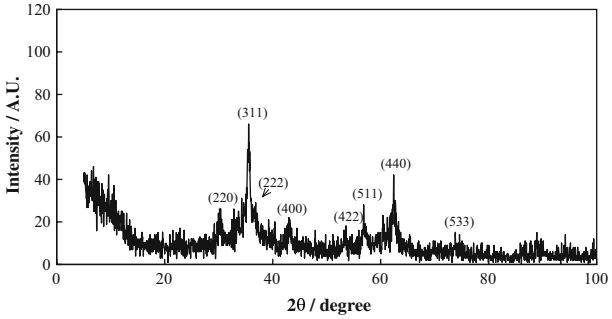

Fig. 1 XRD pattern of dextrin-coated NFNPs

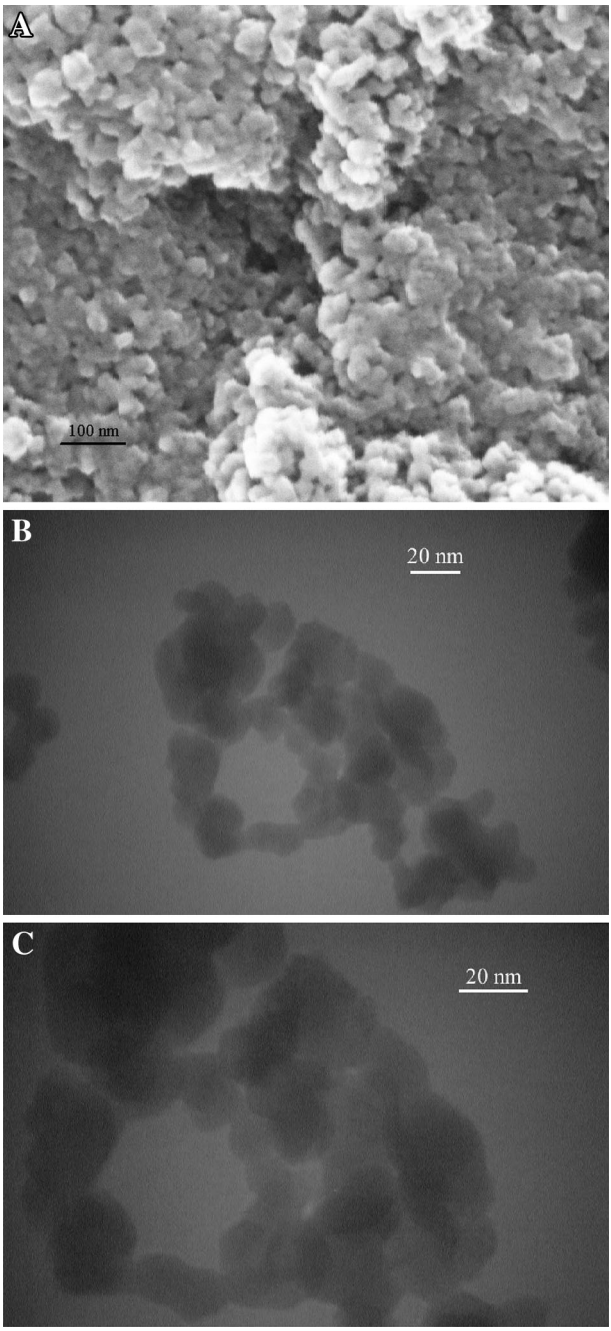

Fig. 2 FESEM (**a**) and TEM (**b**, **c**) images of dextrin-coated NFNPs

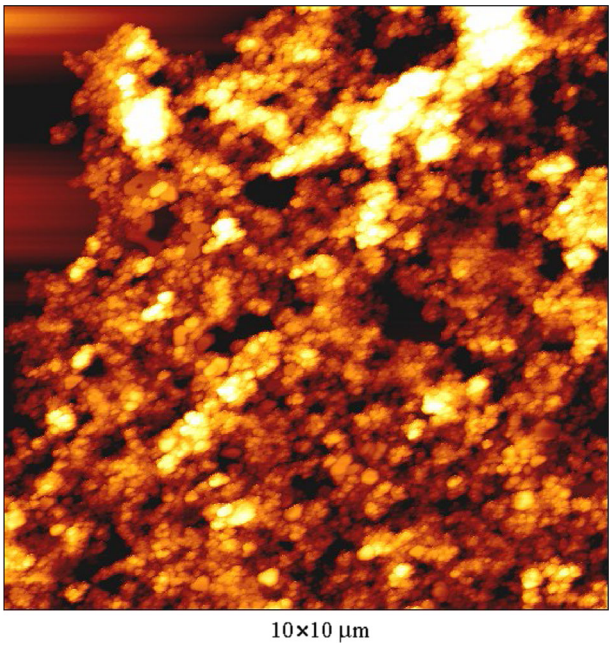

Fig. 3 AFM image of dextrin-coated NFNPs

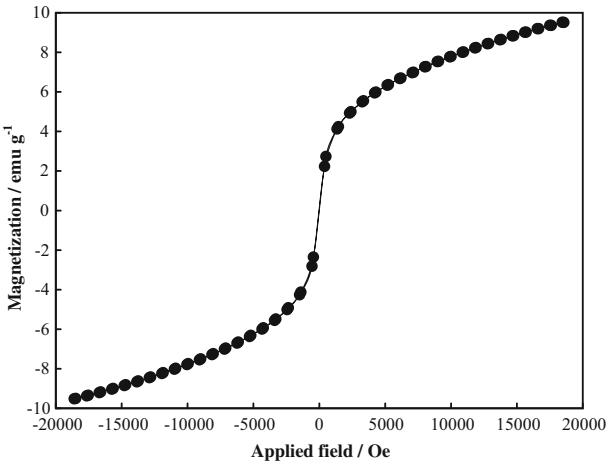

Fig. 4 Magnetization versus applied magnetic field of d-NFNPs at room temperature between −20 and 20 kOe

where n_B is the magnetic moment, M_w is the molecular weight, M_s is saturation magnetization, and the coefficient of 5585 is the magnetic factor. The magnetic properties of d-NFNPs were obtained from hysteresis data and reported in Table 1.

Table 1 Magnetic properties of d-NFNPs obtained from hysteresis data

M_s/emu g^{-1}	H_c/G	M_r/emu g^{-1}	R	n_B
12.3	4.4	23.4×10^{-3}	1.9×10^{-3}	0.52

M_s saturation magnetization, H_c coercivity, M_r remanence magnetization, R remanent ratio $= M_r/M_s$, n_B magnetic moment

The relatively small value of magnetization was related to the dextrin surface coating, and also to the ultra-small size of the NPs [36–38].

NFNPs were synthesized in the presence of dextrin. Dextrin created a shell around NFNPs. An FT-IR spectrum of d-NFNPs is shown in Fig. 5 to characterize the surface nature of d-NFNPs. In this spectrum, the sharp band at around 575 cm^{-1} is due to Fe–O bond [39]. The peak at around 1040 cm^{-1} is attributed to the C–O– or –C–O–C– bonds in dextrin coat. The absorption bond at 2350 cm^{-1} is attributed to C–H bond, and the peaks at around 2928 cm^{-1} are characterized as stretching vibration of $–CH_2$ group of dextrin [22, 34, 39]. In addition, the broad peak around 3381 cm^{-1} is related to the O–H stretching vibration of dextrin. Consequently, it can be concluded that NFNPs were successfully covered with dextrin.

In vitro contrast enhancement of d-NFNPs was detected via measuring relaxivity. Figure 6 shows the signal intensity (SI) of T_2-weighted images (spin–echo pulse sequence, TR = 1800 ms, TE = 88 ms, at room temperature) and T_2^*-weighted images (FLASH pulse sequence, TR = 350 ms, TE = 15 ms) of different concentrations of d-NFNPs in an agar phantom. Signal intensities of T_2 and T_2^*-weighted

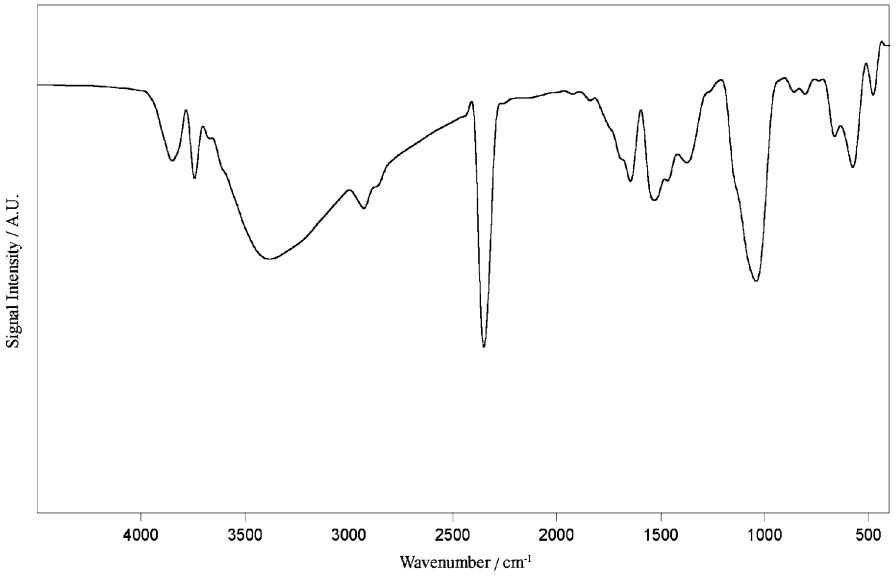

Fig. 5 FT-IR spectrum of dextrin-coated NFNPs

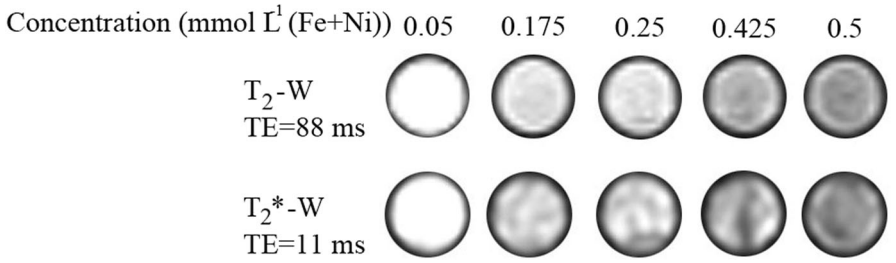

Fig. 6 T_2- and T_2^*-weighted images of dextrin-coated NFNPs at different Fe + Ni concentrations

images increase with increasing NFNPs concentration. This indicates that the magnetic moment of NPs and proton of water interacts suitably, resulting in T_2 and T_2^* shortening. The effectiveness of NPs as contrast agent is detected with relaxivity, which represents the reciprocal of the relaxation time per concentration of metal (Fe + Ni) ions. Changes in T_2 and T_2^* relaxation rates ($1/T_2$ and $1/T_2^*$) as a function of the (Fe + Ni) concentration for d-NFNPs are shown in Fig. 7. Using the following equations:

$$1/T_2 = 1/T_2^0 + r_2(\text{Fe} + \text{Ni}) \tag{2}$$

$$1/T_2^* = 1/T_2^{*0} + r_2^*(\text{Fe} + \text{Ni}) \tag{3}$$

where $1/T_2$ and $1/T_2^*$ are the observed relaxation rates in the presence of d-NFNPs, $1/T_2^0$ ($1/T_2^{*0}$) and r_2 (r_2^*), which are the relaxation rates of pure water (in a solution of NFNPs-free) and transverse relaxivity, respectively. The values of relaxation rates were calculated. The relaxation rates were linearly increased with the (Fe + Ni) concentration. The values of r_2 and r_2^* were obtained as 8.78 and 82.08 mmol L^{-1} - s^{-1}, respectively. The values of r_2^* of d-NFNPs were significantly higher than r_2 that led to strong dark T_2^* MRI signals. Therefore, d-NFNPs are suggested as a potential

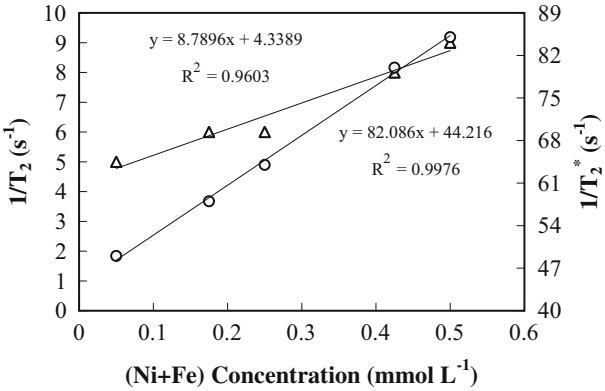

Fig. 7 Dependences of T_2 and T_2^* relaxation rates ($1/T_2$ and $1/T_2^*$) as a function of the (Fe + Ni) concentration for dextrin-coated NFNPs

Table 2 Characteristics of some contrast agents

Contrast agent	Coating material	Size/nm	r_2/mmol L^{-1} s^{-1}	Company
Resovist	Dextran	60	189.0	Schering
Ferumoxytol	Carboxymethyl dextran T_{10}	30	89.0	Advanced magnetic
Endorem/feridex	Dextran T_{10}	120–180	120.0	Guerbet, advanced magnetic
Sinerem/combridex	Dextran T_{10}, T_1	30–15	65.0	Guerbet, advanced magnetic
$Zn_{0.5}Ni_{0.5}Fe_2O_4$	Dextrin	21	8.78	This work

and powerful contrast enhancing agent compared with commercially available iron oxide NPs. A comparison between characteristics of d-NFNPs and some commercially available contrast agents is presented in Table 2.

4 Discussion

Ultra-small size of d-NFNPs (approximately 20 nm) may be very desirable for clinical using. Also, FTIR study confirmed that the surface of NPs is coated with a biocompatible and hydrophilic dextrin layer. Dextrin is a non-toxic material that can be used in vivo. Synthetic magnetic NPs can be used as a diagnosis material in MRI. These materials can be absorbed in cancer cells and make a contrast in SI between normal and malignant cells. Relaxometry and magnetometry study confirm the applicability of the d-NFNPs as a contrast agent in MRI. Although dextrin due to non-magnetic property reduces the magnetization characteristic of the d-NFNPs, relaxometry study shows the utility of d-NFNPs as an MRI contrast agent. In addition, in vitro studies show that the value of r_2^* for d-NFNPs was higher than r_2 and the effectiveness of d-NFNPs as negative contrast agent in the T_2^*-weighted images.

5 Conclusion

In summary, superparamagnetic d-NFNPs were synthesized via simple precipitation technique. d-NFNPs formed spherical structure with 20.5 ± 3.2 nm diameters. This new contrast agent shortens T_2 and T_2^* in MRI imaging, with a relaxivity of 8.78 and 82.08 s^{-1} mmol L^{-1} for r_2 and r_2^*, respectively. These NPs are suitable for T_2^*-weighted MR images. Also, this contrast agent is biocompatible due to d-NFNPs and is proposed for future binding of these NPs to bioactive ligands for target imaging.

Acknowledgments We thank the Research Councils of Shiraz University of Medical Sciences (10064), and the Iran National Science Foundation (INSF) for supporting this research.

Compliance with Ethical Standards

Conflict of interest The authors declare that they have no conflict of interest.

References

1. A. Ito, M. Shinkai, H. Honda, T. Kobayashi, J. Biosci. Bioeng. **100**, 1–11 (2005)
2. Z. Liu, T. Lammers, J. Ehling, Z. Liua, T. Lammersa, J. Ehlinga, S. Fokonga, J. Bornemannc, F. Kiesslinga, J. Gatjensa, Biomaterials **32**, 6155–6163 (2011)
3. H.L. Ma, Y.F. Xu, X.R. Qi, Y. Maitani, T. Nagai, Int. J. Pharm. **354**, 217–226 (2008)
4. S. Sun, C.B. Murray, D. Weller, L. Folks, A. Moser, Science **287**, 1989–1992 (2000)
5. N. Sattarahmady, A. Parsa, H. Heli, J. Mater. Sci. **48**, 2346–2351 (2013)
6. H. Heli, H. Yadegari, A. Jabbari, J. Phys. Chem. **115C**, 10889–10897 (2011)
7. A. Rahi, K. Karimian, H. Heli, Anal. Biochem. **497**, 39–47 (2016)
8. A. Rahi, N. Sattarahmady, H. Heli, Sci. Rep. **5**, Article number 18060 (2015)
9. A. Rahi, N. Sattarahmady, H. Heli, Talanta **156–157**, 218–224 (2016)
10. N. Sattarahmady, H. Heli, R. Dehdari Vais, Biosens. Bioelectron. **48**, 197–202 (2013)
11. N. Sattarahmady, G.H. Tondro, M. Golchin, H. Heli, Biochem. Eng. J. **97**, 1–7 (2015)
12. H. Heli, S. Mirtorabi, K. Karimian, Expert Opin. Ther. Pat. **21**, 819–856 (2011)
13. P. Boisseau, B. Loubaton, C. R. Phys. **12**, 620–636 (2011)
14. R. Lehner, X. Wang, M. Wolf, P. Hunziker, J. Control Release **161**, 307–316 (2012)
15. A.A.M. Elsherbini, M. Saber, M. Aggag, A. El-Shahawy, H.A. Shokier, Magn. Reson. Imaging **29**, 272–280 (2011)
16. H. Heli, N. Sattarahmady, G.R. Hatam, F. Reisi, R. Dehdari Vais, Talanta **156–157**, 172–179 (2016)
17. T.H. Hai, L.H. Phuc, D.T.K. Dung, N.T.L. Huyen, B.D. Long, L.K. Vinh, N.T.T. Kieu, M. Abe, J. Korean Phys. Soc. **53**, 772–775 (2008)
18. M.D. Shultza, S. Calvin, P.P. Fatouros, S.A. Morrison, E.E. Carpenter, J. Magn. Magn. Mater. **311**, 464–468 (2007)
19. D. Pan, S.D. Caruthers, A. Senpan, A.H. Schmieder, S.A. Wickline, G.M. Lanza, Wiley Interdiscip. Rev. Nanomed. Nanobiotechnol. **3**, 162–173 (2011)
20. G.P. Yan, L. Robinson, P. Hogg, Radiography **13**, 5–19 (2007)
21. D.Y. Lee, Macromol. Res. **19**, 843–847 (2011)
22. H.B. Na, I.C. Song, T. Hyeon, Adv. Mater. **21**, 2133–2148 (2009)
23. I. Raynal, P. Prigent, S. Peyramaure, A. Najid, C. Rebuzzi, C. Corot, Invest. Radiol. **39**, 56–63 (2004)
24. K. Niemirowicz, K.H. Markiewicz, A.Z. Wilczewska, H. Car, Adv. Med. Sci. **57**, 196–207 (2012)
25. D. Portet, B. Denizot, E. Rump, J.J. Lejeunea, P. Jallet, J. Colloid Interface Sci. **238**, 37–42 (2001)
26. C. Sciallero, D. Grishenkov, S.V. Kothapalli, L. Oddo, A. Trucco, J. Acoust. Soc. Am. **134**, 3918–3930 (2013)
27. D.K. Kim, Y. Zhang, J. Kehr, T. Klason, B. Bjelke, M. Muhammed, J. Magn. Magn. Mater. **225**, 256–261 (2001)
28. L. Wei, S. Li, J. Yang, Y. Ye, J. Zou, L. Wang, R. Long, O. Zurkiya, T. Zhao, J. Johnson, J. Qiao, W. Zhou, A. Castiblanco, N. Maor, Y. Chen, H. Mao, X. Hu, J.J. Yang, Z.R. Liu, Mol. Imaging Biol. **13**, 416–423 (2011)
29. A.P. Marques, R.L. Reis, J.A. Hunt, Biomaterials **23**, 1471–1478 (2002)
30. W.H. Wong, D.J. Mooney, *in: Synthetic Biodegradable Polymer Scaffolds* (Birkhauser, Boston, 1997), pp. 51–82
31. Q. Xu, Y. Wei, Y. Liu, X. Jia, L. Yanga, M. Gu, Solid State Sci. **11**, 472–478 (2009)
32. J.G. Lee, J.H. Kim, K.P. Chae, J. Korean Phys. Soc. **49**, 604–607 (2006)
33. M. Ahamed, M.J. Akhtar, M.A. Siddiqui, J. Ahmad, J. Musarrat, A.A. Al-Khedhairy, M.S. AlSalhi, S.A. Alrokayan, Toxicology **283**, 101–108 (2010)
34. B. Godbole, N. Badera, S.B. Shrivastava, D. Jaind, L.S.S. Chandrae, V. Ganesanf, Phys. Proc. **49**, 58–66 (2013)
35. P.P. Hankare, R.P. Patil, U.B. Sankpal, S.D. Jadhava, P.D. Lokhandeb, K.M. Jadhavc, R. Sasikalad, J. Solid State Chem. **182**, 3217–3221 (2009)

36. P. Chandrasekharan, D. Maity, C.X. Yong, K.H. Chuang, J. Ding, S.S. Feng, Biomaterials **32**, 5663–5672 (2011)
37. J.M. Jin, *Electromagnetic analysis and Design in Magnetic Resonance Imaging* (CRC Press, Boca Raton, 1998)
38. D. Maity, D.C. Agarwal, J. Magn. Magn. Mater. **308**, 46–55 (2007)
39. J. Varshosaz, H. Sadeghi-aliabadi, S. Ghasemi, B. Behdadfar, Biomed. Res. Int. **2013**, 680712 (2013)